 Human Molecular Genetics, 2000, Vol. 9, No. 2 **195–202**

Discovery and genetic localization of Down syndrome cerebellar phenotypes using the Ts65Dn mouse

Laura L. Baxter, Timothy H. Moran[2], Joan T. Richtsmeier[1], Juan Troncoso[3] and Roger H. Reeves[+]

Department of Physiology and [1]Department of Cell Biology and Anatomy, Johns Hopkins University School of Medicine, 725 North Wolfe Street, Baltimore, MD 21205, USA, [2]Department of Psychiatry and Behavioral Sciences and [3]Department of Pathology, Johns Hopkins University School of Medicine, 720 Rutland Avenue, Baltimore, MD 21205, USA

Received 12 August 1999; Revised and Accepted 12 October 1999

Down syndrome (DS) is the most common genetic cause of mental retardation and affects many aspects of brain development. DS individuals exhibit an overall reduction in brain size with a disproportionately greater reduction in cerebellar volume. The Ts65Dn mouse is segmentally trisomic for the distal 12–15 Mb of mouse chromosome 16, a region that shows perfect conserved linkage with human chromosome 21, and therefore provides a genetic model for DS. In this study, high resolution magnetic resonance imaging and histological analysis demonstrate precise neuroanatomical parallels between the DS and the Ts65Dn cerebellum. Cerebellar volume is significantly reduced in Ts65Dn mice due to reduction of both the internal granule layer and the molecular layer of the cerebellum. Granule cell number is further reduced by a decrease in cell density in the internal granule layer. Despite these changes in Ts65Dn cerebellar structure, motor deficits have not been detected in several tests. Reduction in granule cell density in Ts65Dn mice correctly predicts an analogous pathology in humans; a significant reduction in granule cell density in the DS cerebellum is reported here for the first time. The candidate region of genes on chromosome 21 affecting cerebellar development in DS is therefore delimited to the subset of genes whose orthologs are at dosage imbalance in Ts65Dn mice, providing the first localization of genes affecting a neuroanatomical phenotype in DS. The application of this model for analysis of developmental perturbations is extended by the accurate prediction of DS cerebellar phenotypes.

INTRODUCTION

Trisomy for human chromosome 21 (HSA21), or Down syndrome (DS), is the most common genetic cause of mental retardation, occurring in ~1 in 700 live births (1). Dosage imbalance for the genes on HSA21 affects nearly every organ system in the body, resulting in craniofacial defects, the neurohistopathology of Alzheimer's disease, deficiencies of the immune system, gut abnormalities, abnormalities of dermatoglyphics, hypotonia and cardiac defects (2). Some DS phenotypes, including mental retardation, occur in all affected individuals, whereas other characteristics show variable penetrance. Total brain volume is consistently reduced in DS, with a disproportionately greater reduction in the cerebellum (3,4). This reduction is readily apparent on post-mortem analysis, and has been measured quantitatively by magnetic resonance imaging (MRI) studies reporting a total brain volume of 85% of euploid, and cerebellar volume further reduced to 73% of euploid (5–7).

Experimental approaches to elucidate the mechanisms by which aneuploidy affects development require systematic studies of aneuploid conditions. For DS, significant progress has been made through careful correlation of cytogenetic, molecular and clinical manifestations in individuals with translocations resulting in trisomy for a subset of HSA21 genes (segmental trisomy 21). Maps correlating dosage imbalance of specific regions with specific characteristics provide useful information about segments in which to search for the genes primarily responsible (8,9). Despite these advances, human beings are not the organism of choice to elucidate the relative contributions of HSA21 genes to the DS phenotype. Each individual displays a different subset of the constellation of common DS characteristics, no doubt due in part to the fact that humans are an outbred species, and different genetic backgrounds provide different buffering capacities for specific developmental anomalies. This phenotypic variability means that the absence of a character from an individual with DS is not informative. Combined with the small number of known translocation DS individuals, this variability presents a significant barrier to the resolution attainable by this approach. Another limitation to human studies is that DS is primarily a developmental problem; most consequences of DS are apparent by the time of birth. Systematic studies of embryonic and fetal development are difficult in humans.

Mice provide a powerful experimental system for studies of mammalian aneuploidy (10). Studies of mouse development are advanced, providing a baseline for recognizing aberrant

[+]To whom correspondence should be addressed. Tel: +1 410 955 6621; Fax: +1 410 955 0461; Email: rreeves@welch.jhu.edu

patterns. Genetic background can be defined and controlled using crosses involving highly characterized inbred mouse strains. Detailed analysis of the mouse genome is advancing in step with human genome efforts, providing a wealth of genetic information and reagents for genetic and biological analysis. Mice provide many practical benefits, such as a short generation time, small size, relatively low cost, and accessibility to all tissues at all developmental stages. Technical developments in mouse genetics provide unprecedented approaches to studies of genetic problems. The development of embryonic stem (ES) cell technology provides a unique system in mammals, allowing *in vitro* experimental alterations to be perpetuated through the mouse germ line. Defined gene alterations and even re-engineering of chromosomes using ES cells are becoming routine (11,12).

The Ts65Dn mouse has segmental trisomy for a region of mouse chromosome 16 (MMU16) that exhibits perfect conserved linkage with distal HSA21 (13,14). These mice are at dosage imbalance for the region from *App* through *Tmprss2*, which contains roughly half of the genes on HSA21 (Fig. 1). Ts65Dn mice are not at dosage imbalance for the most distal segment of HSA21, which exhibits conserved synteny with MMU17 and -10. However, the region triplicated in Ts65Dn includes the HSA21 segment from *D21S55* to *MX1*, which has been reported to include genes responsible for many DS traits through assessment of individuals with segmental trisomy 21 (8,9).

The Ts65Dn mouse exhibits a range of phenotypes that are analogous to those seen in DS. In the Morris Swim Maze, the Ts65Dn mouse shows deficits in hippocampal-based spatial learning and memory (15). These results have been replicated and extended to demonstrate a consistent and severe defect in spatial learning (16–20). A slight decrease in the density of the granule cell layer of the dentate gyrus has been reported, a structural defect that may be related to the learning defect (21). Ts65Dn mice also exhibit age-related degeneration of the septo-hippocampal cholinergic neurons, as well as astrocytic hypertrophy (22). A recent study on Ts65Dn demonstrates abnormalities of gut function and metabolism that parallel those seen in DS (23). Detailed analysis of the craniofacial skeleton and neurocranium of Ts65Dn mice demonstrates additional, quantitative phenotypes that parallel those seen in DS (24).

These results suggest that many genetic pathways regulating development in mammals are affected in similar ways in response to the common genetic insult in DS and in Ts65Dn mice. In this study, high resolution MRI and histological analysis were used to quantify changes in the Ts65Dn cerebellum. Ts65Dn mice showed a significant reduction in cerebellar volume paralleling that in DS, and accurately predicted a new cerebellar phenotype confirmed by analysis of DS brains. The predictive value of the Ts65Dn model and the localization of genes affecting this phenotype in DS extend the applications of this and other mouse models to understand the genetic mechanisms that underlie maldevelopment in aneuploidy.

RESULTS

MRI and histological analysis of total cerebellum

High resolution MRI allows precise measurement of volumes, and eliminates artifacts due to dehydration or paraffin embedding that can occur from histological preparation. Brains of 10

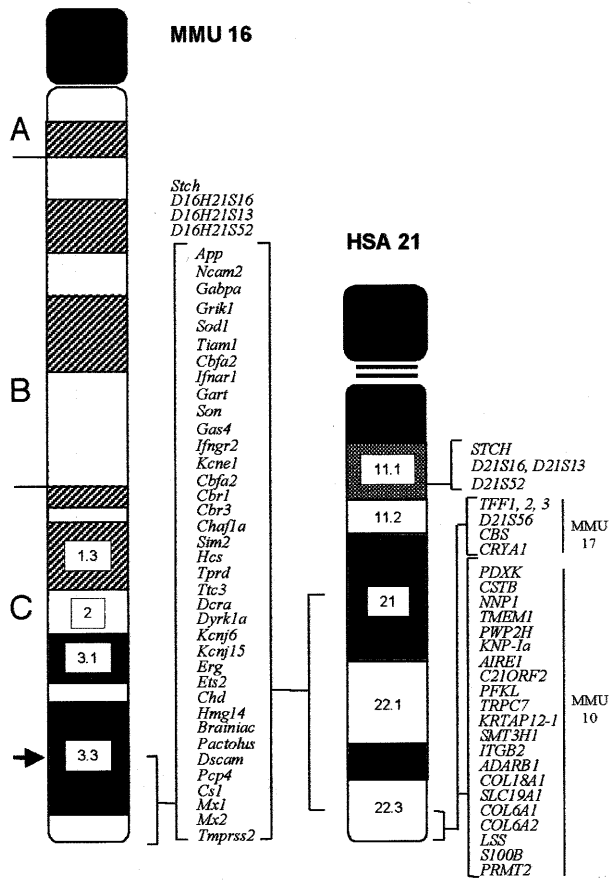

Figure 1. Genes included and excluded from cerebellar phenotypes in Ts65Dn and DS. Known genes that map to the T65Dn translocation chromosome and to HSA21 are shown in brackets adjacent to the cartoon of MMU16, and their cytogenetic locations on MMU16C3.3 and HSA21q21–22.3 are indicated. Those genes shown to the right of HSA21 map outside the T65Dn region of MMU16 or to MMU17 or -10, and thus do not contribute to the cerebellar phenotypes described here. The arrow indicates the T65Dn breakpoint. Major cytological landmarks are indicated on both chromosomes. Comparative map information is from http://www.informatics.jax.org/ and refs 3,36.

Ts65Dn mice and 10 control, euploid littermates were measured with high contrast at very high resolution (isotropic pixel resolution of 125 μm). The architecture of major brain regions (cortex, hippocampus, cerebellum) was clearly defined at this resolution (Fig. 2A). Volumes of total brain, cerebellum and brain excluding cerebellum were determined for each brain in both sagittal and horizontal planes, and these two sets of measurements showed minimal variation (l.8 ± 1.5%). No significant differences due to sex were found in any of the volumetric measurements reported here (data not shown).

Volumes were calculated by summing volumetric pixels (voxels) in every MRI slice. The volume of the Ts65Dn cerebellum was significantly reduced to 88.5% of euploid ($P = 0.015$) (Table 1). The same result was obtained when the measurement was normalized to total brain volume (88.1%, $P = 0.0003$). Normalization to total brain accounts for variation in overall brain size by expressing the cerebellar volume as a fraction of the entire brain, and is commonly used for analysis of human cerebellar volume in DS (5–7). The average volumes of total brain and the brain excluding cerebellum were not significantly different from euploid. Therefore, the

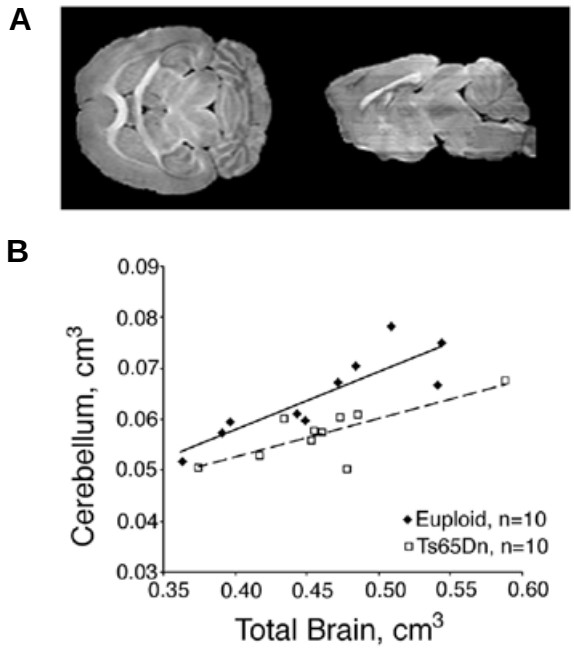

Figure 2. Cerebellar volume is significantly reduced in Ts65Dn mice. (**A**) Representative MRI images in horizontal and sagittal planes (for both views, the rostrum is to the left). (**B**) Bivariate analysis of the volume of the cerebellum relative to total brain volume in Ts65Dn and euploid mice. Reduced major axis regression analysis (37) demonstrates a significant difference between Ts65Dn and euploid ($P = 0.001$).

cerebellum of Ts65Dn mice is specifically reduced in size and is proportionately smaller relative to the total brain size. The degree of reduction showed no significant correlation with age of adult Ts65Dn mice from 3 to 12 months (for Ts65Dn, $r^2 = 0.22$; euploid, $r^2 = 0.078$).

The significant reduction in cerebellar volume due to trisomy was corroborated by measurements of cross-sectional area in histological sections (Fig. 3). Areas of the total brain, cerebellum and brain excluding cerebellum were measured at a midline sagittal section and a para-sagittal section located at the lateral edge of the inferior colliculus. The area of Ts65Dn cerebellum measured on both the midline and lateral sections was significantly reduced. When normalized to total brain, Ts65Dn cerebellum was 81.7% of euploid at the midline and 80.6% of euploid para-sagittally (Table 1). Total brain area showed no significant difference from euploid for either of the measured regions. However, the brain excluding cerebellum was consistently larger than euploid in both area and volumetric measurements, achieving statistical significance at the midline ($P = 0.04$; Table 1). As with volumetric measurements, no differences due to sex were seen in either euploid or segmentally trisomic mice (data not shown).

The thickness of the internal granule layer (IGL) and molecular layer (ML) of the cerebellum was measured to characterize the reduction in cerebellar volume further. The average layer thickness was calculated by dividing the total length of the layer in a midline sagittal section by the total area of the layer. A significant reduction was seen in Ts65Dn in the thickness of both the IGL and the ML (Fig. 4). The Ts65Dn IGL was 86.7% of euploid (Ts65Dn, $n = 6$; euploid, $n = 6$; $P = 0.002$), whereas the molecular layer was 92.3% of euploid ($n = 6$, $P = 0.04$).

Reduced cellular density in the Ts65Dn cerebellum

Reduction in IGL volume of the Ts65Dn cerebellum implies a reduction in the total number of granule cells (GCs). To determine whether cell packing differences in the IGL either compensated for or further reduced GC numbers, cell density was determined by averaging the number of GCs in eight random, non-overlapping 5000 μm^2 fields for each mouse. In Ts65Dn mice, the density of GCs was significantly reduced to 76% of euploid (Ts65Dn, $n = 8$; euploid, $n = 8$; $P = 0.0001$)

Table 1. Cerebellar size in Ts65Dn and euploid mice

	Cerebellum	Total brain	Normalized cerebellum[a]	Brain excluding cerebellum
MRI	Av. volume (cm^3)	Av. volume (cm^3)	Volume	Av. volume (cm^3)
Euploid ($n = 10$)	0.0647	0.4519	0.1412	0.3946
Ts65Dn ($n = 10$)	0.0573	0.4624	0.1245	0.4052
Percent of euploid	88.5	102	88.1	103
P value (*t*-test)	0.015	0.45	0.0003	0.33
Midline histology	Av. area (cm^2)	Av. area (cm^2)	Area	Av. area (cm^2)
Euploid ($n = 8$)	0.0494	0.2976	0.1630	0.2479
Ts65Dn ($n = 7$)	0.0423	0.3118	0.1331	0.2711
Percent of euploid	85.5	105	81.7	109
P value (*t*-test)	0.03	0.15	0.002	0.04
Lateral histology	Av. area (cm^2)	Av. area (cm^2)	Area	Av. area (cm^2)
Euploid ($n = 8$)	0.0364	0.3204	0.1136	0.2831
Ts65Dn ($n = 7$)	0.0298	0.3259	0.0918	0.2953
Percent of euploid	81.9	101	80.6	104
P value (*t*-test)	0.02	0.35	0.008	0.19

[a]For each individual, cerebellar volume or area was divided by the total brain volume or area, respectively. The average of these values is reported.

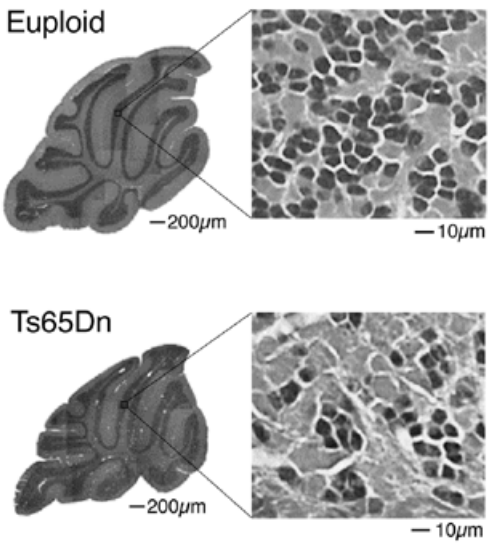

Figure 3. Cerebellar area and granule cell density are reduced in Ts65Dn mice. Images of midline sagittal sections from a Ts65Dn and euploid cerebellum are shown on the left, illustrating the smaller area of cerebellum seen in trisomic mice. The higher magnification views of the granule cell layer on the right show the reduced cellular density in Ts65Dn.

(Fig. 3). There was no significant correlation between age and GC density, suggesting that this is not a function of neurodegeneration throughout adult life (for Ts65Dn, $r^2 = 0.01$; euploid, $r^2 = 0.035$).

Purkinje cells (PCs) are present in a single layer on the surface of the IGL. During development, signals between GCs and PCs are thought to regulate the relative number of each cell type precisely (25). Consistent with this hypothesis and the reduction in GCs, the packing of PCs in Ts65Dn mice, measured as linear density of PCs in histological sections, was reduced to 89.5% of euploid (Ts65Dn, $n = 6$; euploid, $n = 6$; $P = 0.03$) (Fig. 4).

Reduced GC density in the DS cerebellum

The reduction in cerebellar volume in DS is well documented (3–7), but the relative reduction of IGL and ML has not been examined, nor have measurements of cerebellar GC density been reported. Autopsy cerebellar tissue samples were obtained from eight DS and age-matched, euploid control individuals ranging from 2 to 59 years of age. The density of GCs in the IGL was determined for each individual cerebellum by averaging GC number in twelve 5000 μm^2 fields in coronal sections. The cerebellar GC density was significantly reduced in DS individuals to 70% of that in euploid ($P = 0.0002$) (Table 2; Fig. 5). This reduction was significant when all DS brains were compared with all euploid brains, and for the larger groups (age 2–12 and 19–33 years). The older DS adult group (age 58–59 years) was also reduced. However, the two euploid and two DS individuals within this age group did not reach statistical significance, probably due to the small sample size.

Tests of motor function in Ts65Dn mice

The combined reduction in IGL volume (88.5%) and GC density (76%) in Ts65Dn mice predicts a substantial overall reduction in GCs. Given these trisomy-induced changes, motor function was assessed in eight Ts65Dn mice and nine euploid littermate controls using the battery of tests suggested by Crawley and Paylor (26). Tested animals ranged from 3 to 7 months in age and were on the B6/C3H background. Footprint analysis was performed to look for measurable differences in gait length and width. The accelerating rotorod test was used to assess motor coordination and balance. Finally, the mice were tested for both auditory startle and auditory prepulse inhibition, to assess reflex abilities and sensorimotor gating function (27). Ts65Dn mice did not show significant differences from euploid in any of these tests.

DISCUSSION

Several new phenotypes caused by aneuploidy are described in the Ts65Dn mouse. High resolution three-dimensional MRI revealed that the volume of the cerebellum is significantly reduced in mice with segmental trisomy for MMU16. This anatomical phenotype was not readily apparent from previous qualitative analysis (22). Area measurements of histological sections confirmed this result and demonstrated that the IGL and ML are both reduced. The density of GCs and PCs is significantly lower in Ts65Dn mice, and the lower GC density

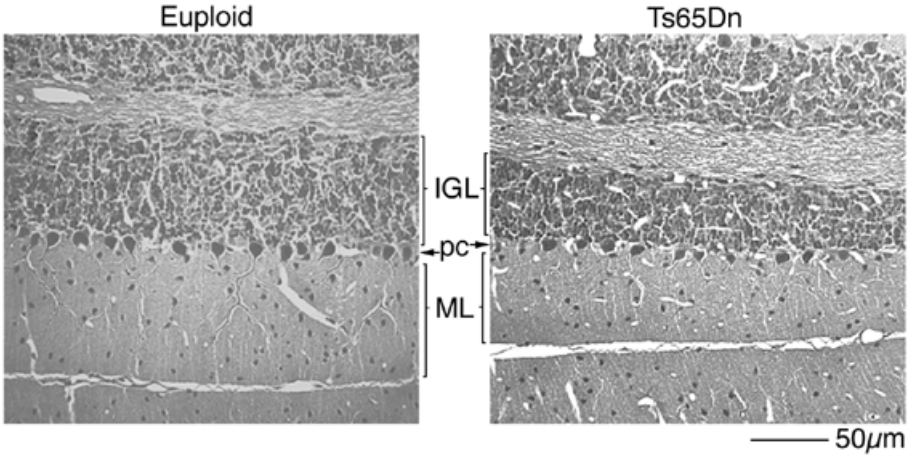

Figure 4. Both the internal granule layer (IGL) and molecular layer (ML) are reduced in Ts65Dn cerebellum. Histological sections of the IGL and ML of representative euploid and Ts65Dn cerebella are shown. These images are taken along the length of folia V, and clearly illustrate the reduced width of the cerebellar layers in Ts65Dn. The reduction in Purkinje cell (pc) linear density is evident here as well.

Table 2. Statistical analysis of granule cell (GC) density in DS and euploid cerebellar samples

	All samples	Age 2–12 years	Age 19–33 years	Age 58–59 years
GC density, euploid	53.6 (7.0, *n* = 8)	57.5 (9.6, *n* = 3)	51 (5.2, *n* = 3)	51.8 (6.2, *n* = 2)
GC density, DS	37.5 (6.6, *n* = 8)	42.2 (6, *n* = 3)	34 (6.4, *n* = 3)	35.8 (6.5, *n* = 2)
Percent of euploid	70	73	67	69
P value (*t*-test)	0.0002	0.04	0.012	0.06

Standard deviations followed by sample sizes are shown in parentheses.

correctly predicted a corresponding reduction in the DS cerebellum. Reduction in cerebellar volume is invariant in DS individuals, and this completely penetrant DS phenotype is accurately recapitulated in the Ts65Dn mouse model. These cerebellar phenotypes provide quantitative endpoints for future studies of gene dosage imbalance in mouse models with smaller, defined segmental trisomies.

No age-related differences in cerebellar structure were seen across the mature adults (3–12 months) analyzed in this study, suggesting that the observed phenotypes are not progressive throughout adulthood. In DS, the reduction in cerebellar volume is apparent by 16 months of age (4), demonstrating that this anomaly arises during development. Availability of brain tissue both pre- and postnatally in Ts65Dn mice will enable detailed examination of the development of the cerebellum in Ts65Dn, and this information will be directly relevant to understanding the reduced size and GC density in cerebellum that occur in DS.

The cerebellar phenotypes observed in Ts65Dn mice paralleled (and predicted) changes in the DS cerebellum. In contrast to the human condition, however, the volume of brain excluding cerebellum was not reduced overall in segmentally trisomic mice. This difference may reflect in part the extensive reductions of cerebral cortex that occur in DS. The much simpler organization of mouse cortex may not be subject to similar reductions as a consequence of trisomy. The occurrence of cerebellar pathology in all individuals on the outbred background on which Ts65Dn mice are maintained indicates that this robust phenotype is a direct consequence of dosage imbalance of a gene or genes on distal MMU16, and not dependent on modifier loci. This result is predicted from the complete penetrance of cerebellar phenotypes in DS.

DS individuals display hypotonia in infancy, a clinical finding that disappears in the first few years of life. Children and adults usually display fine motor deficits that have been variously attributed to problems in cognition or in motor control mechanisms (28). The substantial reduction in cerebellar neurons in Ts65Dn was not reflected in several tests of motor function utilized in this study, consistent with a previous study where Ts65Dn mice showed no deficits in simple sensorimotor tests (19). More sensitive tests of fine motor control are likely to become available in the future, especially as rat paradigms are adapted for use in mice, and these may reveal a phenotype that will provide insights into functional ramifications of this anatomical parallel with DS.

This work provides two substantial contributions to the study of DS. First, clear parallels have been established between anomalous cerebellar development in the Ts65Dn mouse and DS individuals. This includes the description of a new DS phenotype, the significant reduction in cerebellar GC density,

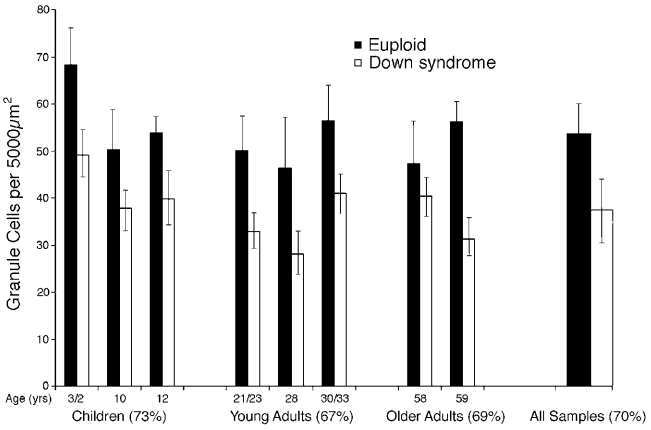

Figure 5. Cerebellar granule cell density is significantly reduced in DS. The values are the averages of cell counts in 12 random, non-overlapping 5000 μm² fields in the granule cell layer. Each bar represents a single individual and the numbers below each bar indicate the age of the individual. When a single age is indicated, both the euploid and DS individual were the same age. Average DS granule cell densities are given as percent of euploid for each group (in parentheses). Granule cell density values were calculated using Abercrombie's correction factor (see Materials and Methods).

reported for the first time in both Ts65Dn and DS individuals. Secondly, Ts65Dn mice are trisomic for only a subset of the genes found on human HSA21. These results therefore delimit the region of HSA21 containing a gene or genes responsible for the DS cerebellar phenotype, providing the first genetic localization of a neuroanatomical trait in DS or Ts65Dn. Inherent strengths of the mouse system include access to all tissues pre- and postnatally, control of genetic background and environment, the possibility for experimental intervention, and the generation of any number of individuals for specific studies. Analysis of the Ts65Dn mouse model will provide direct insights into mechanisms of gene dosage imbalance that produce the cerebellar phenotypes in DS.

MATERIALS AND METHODS

Mice

All mice were obtained from the Jackson Laboratory (Bar Harbor, ME) and maintained in the Johns Hopkins virus- and antibody-free facility with food and water *ad libitum*. For this study, outbred Ts65Dn (B6EiC3H-a/A-Ts65Dn) females were crossed with (B6 × C3H)F_1, CBA/CaJ or (A/J × CBA/J)F_1 male mice. All mice were adults, ranging from 4 to 12 months old. Ploidy was determined by karyotyping cultured peripheral

lymphocytes (29). For MRI analysis, three trisomic and three control mice had a mixed background of CBA and B6/C3H, whereas the remaining seven mice of each group had a B6/C3H background. No differences were attributable to genetic background. For behavioral testing, mice 3–7 months old with the B6/C3H background were used, and were verified by polymerase chain reaction analysis to be negative for retinal degeneration (30). Mice do not show sexual dimorphism in adult brain volume in the strains used (31). Comparison of male and female results confirmed the absence of a sex effect on all phenotypes assessed in this study.

Perfusion and fixation

Mice were deeply anesthetized with methoxyfluorane (Metofane), and perfused intra-cardially with 30 ml of phosphate-buffered saline (PBS) with heparin (50 U/ml), followed by perfusion with 30 ml of ice-cold 4% paraformaldehyde in phosphate buffer. The head was removed and post-fixed overnight in 4% paraformaldehyde at 4°C. The brain was removed the following day, and fixative was cleared from the brain by serial washes in PBS over several days. Fixed brains were stored in PBS at 4°C.

MRI analysis

Fixed Ts65Dn and euploid brains were used for MRI analysis. MRI images of mouse brains were obtained using a 400 MHz General Electric Omega nuclear magnetic resonance spectrometer interfaced to a 9.4 T/89 mm vertical bore magnet equipped with Accustar actively shielded gradients capable of developing gradient strengths up to 1400 mT/m. A three-dimensional spin echo imaging sequence with an echo time of 32 ms and a recycle delay of 1 s was employed. The radio frequency (RF) probe consisted of a cylindrical loop gap resonator (dimensions: 16 mm length, 12 mm diameter) made of copper foil. Adiabatic RF pulses of 1 ms duration were employed for uniform excitation across the sample. Because the brains were suspended in PBS for analysis, the water signal from the buffer was minimized by applying diffusion gradients (200 mT/m for 3 ms along *x* and *z* directions) symmetrically on both sides of the re-focusing pulse. The data matrix size was $128 \times 128 \times 64$ voxels and the corresponding field of view was $16 \times 16 \times 8$ mm, yielding isotropic pixel resolution of 125 μm. The investigator was blinded to the sample genotypes for both MRI collection and data analysis (see below).

The resulting MRI images were analyzed using the BrainImage program (v2.2.4, 1999; A.L. Reiss, Stanford University Psychiatry Neuroimaging Laboratory), an imaging program derived from NIH Image that retains general digital image processing features, but is also specialized to analyze brain images, specifically MRI files. BrainImage allows visualization and measurement of MRI data in three dimensions in any plane of section desired, thus allowing precise alignment of the brains for uniform analysis among all samples. Volumetric measurements were taken of cerebellum, brain excluding cerebellum and total brain. Olfactory bulbs, brain stem posterior of the cerebellum and ventricular space were excluded in volumetric measurements. Brain regions were defined manually, using atlases of the mouse and rat brain for reference (32,33). Target regions were defined in each slice, then the area of each region was calculated. These areas were converted to volumes for each slice, then summed for the whole brain to give total volume. Brains were measured in both the sagittal and horizontal planes, providing two measured values for each region and minimizing error in defining the boundaries of the cerebellum due to angle of view. Calculated values for each of these regions were obtained by subtraction from the total brain measurements. These four volumetric measurements (two measured, two calculated) were averaged, giving four measurements for each region. Statistical calculation of *P* values (for MRI and all subsequent data analysis) was performed using Student's *t*-test. Comparison of results from males and females demonstrated no differences in any parameter (data not shown).

Histological analysis

All histological samples were processed according to standard protocols. Dissected mouse brains were fixed in 4% paraformaldehyde, dehydrated by a series of ethanol washes of increasing ethanol concentration, cleared using Histoclear (VWR, West Chester, PA), infused with paraffin at 55°C, and embedded in the sagittal orientation. Five micrometer serial sections were taken which spanned the midline and extended ~2 mm laterally.

Human cerebella were fixed on autopsy in 10% neutral buffered formalin no more than 26 h post-mortem, and cut coronally after 2 weeks. Tissue blocks were dehydrated, embedded in paraffin and cut in 5 μm sections. None of the tissue samples exhibited signs of GC autolysis. Both mouse and human brain sections were stained with hematoxylin and eosin.

For low magnification imaging of total mouse brain sections, digital images were made using a UMAX PowerLook II scanner at 1200 d.p.i. resolution. As for MRI measurements, the olfactory bulbs, brain stem posterior to the cerebellum and ventricular spaces were excluded. For high magnification imaging of the cerebellum (for mouse and human), sections were viewed using a Zeiss Axiophot Microscope, and digitally captured using a Hitachi HV-C10 CCD Camera and the Metamorph imaging program (Universal Imaging, West Chester, PA). All images were analyzed using the BrainImage program. Comparison of results from males and females demonstrated no differences in any parameter (data not shown).

To obtain the average width of the IGL and ML, the length of the layer in a whole mid-sagittal section (measured along the center of the IGL) was divided by the total area of the layer, yielding an average layer width. The PC layer was not distinguished from the ML, and therefore was included in the estimation of ML width. For GC counting in murine and human cerebellum, cells were counted within a 5000 μm^2 area of the GC layer. Eight independent, non-overlapping fields were selected randomly along the length of folias V, VI and VII in each mouse brain, and the number of GCs were counted within each field and averaged to calculate density for each sample. For human GC density, the same technique was employed, but 12 fields were counted for each human sample along the lengths of various folia of the cerebellum. Regions sampled were limited by the availability of tissue, but this technique of random sampling is supported by data reporting uniform GC density throughout the human cerebellum (34). For mouse brains, cells were counted in mid-sagittal and para-sagittal sections, from which area was measured.

Although all cell counts are presented as relative values rather than absolute values, Abercrombie's correction factor was used for the purpose of calculating GC density: $P = A[M/(L + M)]$, where P is estimated cell number, A is nuclear count, M is section thickness in micrometers (5 μm for this analysis) and L is average nuclear diameter (35). For Purkinje cell counting, the total number of PCs in a midline sagittal section was counted and divided by the length of the Purkinje layer, giving a linear density.

Motor function

Mice were tested on an accelerating rotorod (Economex; Columbus Instruments, Columbus, OH) twice per day for 4 days with a 3 h rest period between trials. The rotorod accelerated gradually from 5 to 50 r.p.m. over a 4 min trial period. The latency to fall off the rod was the dependent variable for each trial and improvement in performance was tracked across days (26).

For footprint analysis, the hindpaws of the mice were coated with red ink, and the mice were allowed to walk along a 5 cm wide corridor lined with paper. The average length and width between pawprints were measured for each mouse and differences in variability were analyzed using ANOVA.

For both auditory startle and prepulse inhibition, mice were tested in an SR-Lab Systems chamber (San Diego Instruments, San Diego, CA) according to the method of Paylor and Crawley (27). Mice were placed in a plexiglass cylinder (5.1 cm outside diameter) mounted on a platform with a piezoelectric accelerometer unit attached below the chamber. The piezoelectric unit transduced vibrations into signals that were rectified and stored by a computer interface. The cylinder and platform were located in a sound-attenuated chamber with a loudspeaker 28 cm above the cylinder. The sensitivity of the unit was calibrated using a vibrating standardization unit. For auditory startle, test sessions consisted of a 5 min adaptation period followed by assessment of responses to auditory stimuli. The background noise level in the chamber was 70 dB. Each subject was presented 36 trials over a 9 min test session, and nine different sound levels (70, 74, 78, 82, 86, 90, 100, 110 and 120 dB) were presented four times in a semi-random sequence for a 40 ms duration. Maximum startle amplitude recorded during a 65 ms sampling interval was the dependent variable. The magnitude of startle was compared with the response following the 70 dB stimulus. The threshold was defined as the stimulus level that produced a significantly higher response than the 70 dB sound. The maximum startle amplitudes were also compared.

For prepulse inhibition, test sessions consisted of a 5 min acclimation period, followed by 42 trials over a 10.5 min test session. Each session consisted of seven trial types presented in semi-random fashion: a 40 ms 120 dB burst of sound, no stimulus and five different acoustic prepulse stimulus trials (74, 78, 82, 86 or 90 dB) presented so that the onset of the prepulse occurred 100 ms prior to the onset of the startle stimulus. The maximum startle amplitude recorded during a 65 ms sampling interval was the dependent variable.

ACKNOWLEDGEMENTS

The authors would like to thank Vadappuram Chacko for innovative development of the MRI scanning protocols, and Allan Reiss and Mike Abrams for generous assistance with BrainImage. This work was supported by a National Science Foundation graduate fellowship (L.L.B.), and by PHS awards AG05146 (J.T.) and HD24605 (R.H.R.).

REFERENCES

1. Hook, E.B. (1981) Down syndrome frequency in human populations and factors pertinent to variation in rates. In de la Cruz, F.F. and Gerald, P.S. (eds), *Trisomy 21 (Down Syndrome): Research Perspectives*. University Park Press, Baltimore, MD, pp. 3–68.
2. Coyle, J.T., Oster-Granite, M.L. and Gearhart, J.D. (1986) The neurobiologic consequences of Down syndrome. *Brain Res. Bull.*, **16**, 773–787.
3. Davidoff, L.M. (1928) The brain in mongolian idiocy. *Arch. Neurol. Psychiatr.*, **20**, 1229–1257.
4. Crome, L., Cowie, V. and Slater, E. (1966) A statistical note on cerebellar and brain stem weight in mongolism. *J. Ment. Defic. Res.*, **10**, 69–72.
5. Aylward, E.H., Habbak, R., Warren, A.C., Pulsifer, M.B., Barta, P.E., Jerram, M. and Pearlson, G.D. (1997) Cerebellar volume in adults with Down syndrome. *Arch. Neurol.*, **54**, 209–212.
6. Jernigan, T.L. and Bellugi, U. (1990) Anomalous brain morphology on magnetic resonance images in Williams syndrome and Down syndrome. *Arch. Neurol.*, **47**, 529–533.
7. Raz, N., Torres, I.J., Briggs, S.D., Spencer, W.D., Thornton, A.E., Loken, W.J., Gunning, F.M., McQuain, J.D., Driesen, N.R. and Acker, J.D. (1995) Selective neuroanatomic abnormalities in Down's syndrome and their cognitive correlates: evidence from MRI morphometry. *Neurology*, **45**, 356–366.
8. Delabar, J.M., Theophile, D., Rahmani, Z., Chettouh, Z., Blouin, J.L., Prieur, M., Noel, B. and Sinet, P.M. (1993) Molecular mapping of twenty-four features of Down syndrome on chromosome 21. *Eur. J. Hum. Genet.*, **1**, 114–124.
9. Korenberg, J.R., Chen, X.N., Schipper, R., Sun, Z., Gonsky, R., Gerwehr, S., Carpenter, N., Daumer, C., Dignan, P., Disteche, C. *et al.* (1994) Down syndrome phenotypes: the consequences of chromosomal imbalance. *Proc. Natl Acad. Sci. USA*, **91**, 4997–5001.
10. Kola, I. and Herzog, P. (1997) Animal models in the study of the biological function of genes on human chromosome 21 and their role in the pathophysiology of Down syndrome. *Hum. Mol. Genet.*, **6**, 1713–1727.
11. Ramirez-Solis, R., Liu, P. and Bradley, A. (1995) Chromosome engineering in mice. *Nature*, **378**, 720–724.
12. Bradley, A. and Liu, P. (1996) Target practice in transgenics [news]. *Nature Genet.*, **14**, 121–123.
13. Davisson, M.T., Schmidt, C., Reeves, R.H., Irving, N.G., Akeson, E.C., Harris, B.S. and Bronson, R.T. (1993) Segmental trisomy as a mouse model for Down syndrome. *Prog. Clin. Biol. Res.*, **384**, 117–133.
14. Reeves, R.H. and Cabin, D.E. (1999) Mouse chromosome 16. *Mamm. Genome*, **10**, 957.
15. Reeves, R.H., Irving, N.G., Moran, T.H., Wohn, A., Kitt, C., Sisodia, S.S., Schmidt, C., Bronson, R.T. and Davisson, M.T. (1995) A mouse model for Down syndrome exhibits learning and behaviour deficits. *Nature Genet.*, **11**, 177–184.
16. Demas, G.E., Nelson, R.J., Krueger, B.K. and Yarowsky, P.J. (1996) Spatial memory deficits in segmental trisomic Ts65Dn mice. *Behav. Brain Res.*, **82**, 85–92.
17. Demas, G.E., Nelson, R.J., Krueger, B.K. and Yarowsky, P.J. (1998) Impaired spatial working and reference memory in segmental trisomy (Ts65Dn) mice. *Behav. Brain Res.*, **90**, 199–201.
18. Escorihuela, R.M., Fernandez-Teruel, A., Vallina, I.F., Baamonde, C., Lumbreras, M.A., Dierssen, M., Tobena, A. and Florez, J. (1995) A behavioral assessment of Ts65Dn mice: a putative Down syndrome model. *Neurosci. Lett.*, **199**, 143–146.
19. Escorihuela, R.M., Vallina, I.F., Martinez-Cue, C., Baamonde, C., Dierssen, M., Tobena, A., Florez, J. and Fernandez-Teruel, A. (1998) Impaired short- and long-term memory in Ts65Dn mice, a model for Down syndrome. *Neurosci. Lett.*, **247**, 171–174.
20. Coussons-Read, M.E. and Crnic, L.S. (1996) Behavioral assessment of the Ts65Dn mouse, a model for Down syndrome: altered behavior in the elevated plus maze and open field. *Behav. Genet.*, **26**, 7–13.
21. Insausti, A.M., Megias, M., Crespo, D., Cruz-Orive, L.M., Dierssen, M., Vallina, T.F., Insausti, R. and Florez, J. (1998) Hippocampal volume and neuronal number in Ts65Dn mice: a murine model of Down syndrome. *Neurosci. Lett.*, **253**, 175–178.

22. Holtzman, D.M., Santucci, D., Kilbridge, J., Chua-Couzens, J., Fontana, D.J., Daniels, S.E., Johnson, R.M., Chen, K., Sun, Y., Carlson, E. *et al.* (1996) Developmental abnormalities and age-related neurodegeneration in a mouse model of Down syndrome. *Proc. Natl Acad. Sci. USA*, **93**, 13333–13338.
23. Cefalu, J.A., Croom Jr, W.J., Eisen, E.J., Jones, E.E., Daniel, L.R. and Taylor, I.L. (1998) Jejunal function and plasma amino acid concentrations in the segmental trisomic Ts65Dn mouse. *Growth Dev. Aging*, **62**, 47–59.
24. Richtsmeier, J.T., Baxter, L.L. and Reeves, R.H. (2000) Parallels of craniofacial maldevelopment in Down syndrome and Ts65Dn mice. *Dev. Dynam.*, in press.
25. Herrup, K. and Sunter, K. (1987) Numerical matching during cerebellar development: quantitative analysis of granule cell death in staggerer mouse chimeras. *J. Neurosci.*, **7**, 829–836.
26. Crawley, J.N. and Paylor, R. (1997) A proposed test battery and constellations of specific behavioral paradigms to investigate the behavioral phenotypes of transgenic and knockout mice. *Horm. Behav.*, **31**, 197–211.
27. Paylor, R. and Crawley, J.N. (1997) Inbred strain differences in prepulse inhibition of the mouse startle response. *Psychopharmacology (Berlin)*, **132**, 169–180.
28. Latash, M.L. and Corcos, D.M. (1991) Kinematic and electromyographic characteristics of single-joint movements of individuals with Down syndrome. *Am. J. Ment. Retard.*, **96**, 189–201.
29. Davisson, M.T. and Akeson, E.C. (1987) An improved method for preparing G-banded chromosomes from mouse peripheral blood. *Cytogenet. Cell Genet.*, **45**, 70–74 [Erratum (1988) *Cytogenet. Cell Genet.*, **48**, 192].
30. Pittler, S.J. and Baehr, W. (1991) Identification of a nonsense mutation in the rod photoreceptor cGMP phosphodiesterase β-subunit gene of the *rd* mouse. *Proc. Natl Acad. Sci. USA*, **88**, 8322–8326.
31. Goffinet, A. and Rakic, P. (2000) *Mouse Brain Development.* Springer, Berlin, Germany, in press.
32. Paxinos, G. and Watson, C. (1986) *The Rat Brain in Stereotaxic Coordinates.* Academic Press, New York, NY.
33. Slotnik, B.M. and Leonard, C.M. (1975) *A Stereotaxic Atlas of the Albino Mouse Forebrain.* US Department of Health, Education and Welfare, Rockville, MD.
34. Andersen, B.B., Korbo, L. and Pakkenberg, B. (1992) A quantitative study of the human cerebellum with unbiased stereological techniques. *J. Comp. Neurol.*, **326**, 549–560.
35. Abercrombie, M. (1946) Estimation of nuclear population from microtome sections. *Anat. Rec.*, 239–247.
36. Wiltshire, T., Pletcher, M., Cole, S.E., Villanueva, M., Birren, B., Lehoczky, J., Dewar, K. and Reeves, R.H. (1999) Perfect conserved linkage across the entire mouse Chromosome 10 region homologous to human Chromosome 21. *Genome Res.*, **9**, in press.
37. Clarke, M.R.B. (1980) The reduced major axis of a bivariate sample. *Biometrika*, **67**, 441–446.